RSC Advances

ROYAL SOCIETY OF CHEMISTRY

www.rsc.org/advances

Interconnected PVDF-CTFE hydrophobic membranes for MD desalination: Effect of PEGs on phase inversion process

Libing Zheng[a, b], Jun Wang[a, b*], Yuansong Wei[a, b], Yong Zhang[a, b], Kun Li[a,b], Zhenjun Wu[c]

a. Key Laboratory of Drinking Water Science and Technology, Research Center for Eco-Environmental Sciences, Chinese Academy of Sciences, Beijing, 100085, China; b. Beijing Key Laboratory of Industrial Wastewater Treatment and Reuse, Research Center for Eco-Environmental Sciences, Chinese Academy of Sciences, Beijing, 100085, China;c. School of Chemical & the Environment, Beijing Institute of Technology, Beijing, 100085, China

** Corresponding author:*

Jun Wang, Tel.: +86-10-62917207; Fax: +86-10-62917207. E-mail address: *junwang@rcees.ac.cn,* 18 Shuangqing Road, Haidian District, Beijing 100085, China.

ABSTRACT

In this work, poly (vinylidene fluoride-co-chlorotrifluoroethylene) (PVDF-CTFE) was used for hydrophobic membranes preparation by the non-solvent induced phase inversion (NIPS) technique. The effects of poly (ethylene glycol) (PEG) molecular weight and dosage were investigated in terms of the membrane morphology, contact angle, surface free energy, and membrane pore structure for both surface pores and overall pores. All membranes possessed typical liquid-liquid demixing asymmetric structure and the contact angles were higher than 85°. Furthermore, increasing the PEG molecular weight and dosage significantly altered the membrane pore structure and surface roughness as a result of the variation of the phase inversion process. The solid-liquid demixing was responsible for the variation of membrane morphology, pore structure, hydrophobicity, and DCMD performance as PEGs with higher molecular weight or dosage was added. The PVDF-CTFE membranes were suitable for MD application for the high hydrophobicity, small pore size with narrow pore distribution, high DCMD performance, especially the interconnected pore structure. The membrane containing 5 wt. % PEG-400 was evidenced to be the optimal one for the MD process, mainly according to the high interconnected pore structure which provide more passages for vapour transfer. The permeate flux was 17.98 kg/(m^2.h) with a conductivity as low as 7 μS/cm at the temperature difference of 30ºC. In addition, an excellent performance sustainability was observed including a relatively steady permeate flux and conductivity during the 360 hrs continuous DCMD operation.

Keywords: PVDF-CTFE; Phase inversion; PEGs; DCMD; Hydrophobic membrane.

1. Introduction

Fresh water scarcity and contamination is one of major global challenges of our time. Desalination of seawater and brackish water is a feasible approach to alleviate this issue. Currently, thermal-based distillation or membrane separation technologies are commonly applied for desalination applications, multi-stage flash evaporation (MSF), multi-effect distillation (MED), and reverse osmosis (RO) comprise almost 93% of the total world installed desalination capacity[1-5]. Membrane distillation (MD), a thermally-driven separation process combining the thermal and membrane processes[6, 7], has been widely studied for seawater or brackish water desalination in lab-scale. The driving force in MD is the vapour pressure difference induced by the temperature difference across the membrane, which only allows for the transportation of vapour molecules. As a result, high salt rejection can be envisioned even under low operation pressure and temperature, presenting tremendous advantages over conventional thermal- or membrane-based desalination processes[8, 9].

The preparation of an appropriate membrane for MD presents a great challenge for both academia and industry. The membranes need to be hydrophobic and possess appropriate pore structure and morphology. In addition, excellent mechanical and chemical stability is also required to maintain a stable performance[10]. PVDF is currently considered to be the most suitable polymer due to its excellent hydrophobicity and processability compared to other hydrophilic membrane materials

such as polyethylene (PE), polypropylene (PP), and polytetrafluoroethylene (PTFE)[7, 11, 12]. However, hydrophobic PVDF membranes still facing many technical limitations impeding its further application, which mainly related to its low mechanical strength, hydrophobicity and permeate flux. In this regard, efforts have been dedicated to the search of alternative materials for membrane fabrication and the improvement in membrane preparation process, as well as the development of composite membrane and nano-composite membrane[13-16]. The PVDF-based copolymer, which possesses higher hydrophobicity due to its high fluorine content, attracted considerable attention as an alternative choice for hydrophobic membrane preparation[12]. Poly (vinylidene fluoride-co-tetrafluoroethylene) (PVDF-TFE), poly (vinylidene fluoride-co-trifluoroethylene) (PVDF-TrFE), poly (vinylidene fluoride-co-hexafluoropropylene) (PVDF-HFP) and few other PVDF-based graft copolymers have been used in hydrophobic membrane preparation[17].

PVDF-CTFE is another commercial fluoropolymer which possess excellent mechanical strength, high hydrophobicity, and good chemical and thermal stability due to the presence of C-F bond[12, 18]. And it can be easily grafted via atom transfer radical polymerization (ATRP) owing to the CTFE segment. Thus, it has been employed for membrane preparation through either NIPS[19-24] or electro-spinning processes[25, 26]. However, to the best knowledge of the authors, the natural hydrophobicity of PVDF-CTFE was largely overlooked, and a systematic study of PVDF-CTFE hydrophobic membrane preparation is desperately needed. In this

regard, it is of great interests to study the use of PVDF-CTFE copolymer for hydrophobic membrane preparation and its potential application in MD. It was confirmed that PVDF-CTFE copolymer has several competitive advantages over other PVDF homopolymers and as well as great potentials for hydrophobic membrane fabrication in a previous study[27].

NIPS is commonly applied for polymeric membrane preparation, in which the phase inversion process was easily influenced by many factors and led to membrane with various morphology and pore structure. Additives has been widely used to fine-tune the membrane morphology and permeability based on this knowledge. It could not only alters the solvation power of the solvent, but also affects the phase inversion process both thermodynamically and kinetically[28]. PEG is one of the most commonly used additive, which has been studied in both hydrophilic and hydrophobic membrane preparation[29-32]. It was reported that when using PEG as additive, its molecular weight and dosage showed great but diversified impact on membrane properties[33-35]. As the same additive may even show entirely different effects on different multi-component polymer solution systems, its effect on PVDF-CTFE hydrophobic membrane preparation should carefully concerned as PEGs was used as additives.

In this study, PVDF-CTFE copolymer was used for hydrophobic membrane preparation. The objective was to tune the membranes by the addition of PEGs with

different molecular weight and dosage. Membranes morphology, surface and overall pore structure, porosity, and hydrophobicity were studied to demonstrate the influence of PEG additives form the perspective of variation in phase inversion process. The permeability of resultant membranes was investigated by DCMD test, and a 360 hrs continuous DCMD test was also carried out to investigate the membrane sustainability.

2. Material and methods

2.1 Materials

Commercial PVDF-CTFE copolymer powder (Solef®, 32008) was purchased from Solvay (Belgium) and was dried at 50ºC for 24 hours before use. DMAc (>99%) was obtained from Shanghai Jingwei Chemical Co., Ltd. (Shanghai, China). PEGs with molecular weights ranging from 200 to 2000 Da were supplied by Tianjin Guangfu Research Institute of Fine Chemical Engineering (Tianjin, China). Porefil® liquid used as the wetting fluid was purchased by Porometer (Eke, Belgian). Ethanol (GR grade, 99.9%), NaCl (GR grade, 99.5%), glycerol (AR, 99%), and diiodomethane (CP) were all purchased from Beijing Chemical works (Beijing, China). Deionized water was used as coagulant for membrane preparation.

2.2 Membrane preparation

Pre-dried PVDF-CTFE copolymer powder, DMAc and pre-designed amounts of PEGs with different molecular weights were mixed in a sealed flask and stirred at 30° C for 24 hrs to obtain a homogeneous polymer solution (detailed was shown in Table

1). For all casting solutions, the polymer concentration was 12 wt.%. The homogeneous polymer solution was then allowed for degassing in a vacuum oven at 30ºC for 24 hrs.

Table 1

Flat sheet PVDF-CTFE hydrophobic membranes were prepared by the dry-wet phase inversion method (also known as NIPS). Prior to membrane casting a piece of hydrophilic PET nonwoven fabric, which function as the supporting layer to prevent membrane shrinking and enhance membrane mechanical strength, was attached on a spotless flat glass plate. The casting solution was subsequently cast uniformly on the surface of the supporting layer by a casting knife with a gap of 0.25 mm. After exposing in air for 15s, the film was immersed into a deionized water bath at 25° C. The prepared nascent membranes were then removed from the coagulation bath and washed with running water to remove the residual additives and solvent. Finally, the wet membranes were air dried at room temperature and stored for subsequent measurement and testing.

2.3 Membrane morphology

The membrane surface and cross-section morphologies were observed using a HITACHI SU8020 field emission scanning electron microscope (FE-SEM) (Hitachi, Japan). The FE-SEM was operated under standard high-vacuum conditions at 3.00 kV. The samples for cross-section observation were firstly frozen in liquid nitrogen for cryogenic fracturing to maintain the pore structure. All the samples were sputtered

with gold nanoparticles under vacuum with a HITACHI E-1010 Ion Sputtering device (Hitachi, Japan) prior to SEM observation.

2.4 Membrane surface morphology and pore structure

As topography would affect the brightness in SEM images, it can be used to indicate the state of membrane surface[36, 37]. Membrane coupons with a size of 12.7×8.8 μm was scanned using SEM and the 10,000× magnified images were obtained and be further analysed using the image-pro-plus 6.0 software. The pore size, surface porosity, pore roundness, and the SEM roughness index[38] were calculated to understand the surface pore structure, and the detailed methods were shown in the *Supporting Information*. The grayscale histograms and three dimension (3-D) morphology was obtained by image J software as described in previous works[39, 40], and the method was shown in the *Supporting Information*.

2.5 Porosity, pore size and pore size distribution

The overall porosity of the membrane was defined as the volume proportion of the pores over the total volume of the membrane, gravimetric method was applied to determine the porosity. The membrane sample was tore apart off from the nonwoven fabric supporting layer and immersed in ethanol solution and ultrapure water for each 24 hrs to fill the membrane pores with ethanol and then replace it with ultrapure water. Finally, the wet membranes and dried membrane were weighed, and the membrane porosity (ε) was calculated by the following equation:

$$\varepsilon = \frac{(M_w - M_d)/\rho_w}{(M_w - M_d)/\rho_w + M_d/\rho_p} \quad (1)$$

Where M_w is the weight of the wet membrane, M_d is the weight of the dry membrane, ρ_w and ρ_p are the density of water and membrane, respectively.

Apart from the porosity measurement, the bubble point, pore size and pore size distribution of the flat sheet membranes were also investigated by gas-liquid displacement method using a Capillary Flow Porometer Porolux 1000 (Porometer, Belgium) to study the effects of PEGs on the permeation properties as described in other work[41]. The gas flux percentage was plotted against the pore size to represent the percentage of the corresponding pores.

2.6 Membrane hydrophobicity

The contact angles of membranes with 3 liquids with different polarity (i.e., deionized water, glycerol, and diiodomethane) were measured to evaluate the membranes hydrophobicity using an OCA 15EC Video-Based Contact Angle Meter (Data Physics, Germany). Five different positions of each membrane sample were measured and the average value was reported with the standard deviation.

The membrane surface free energy was calculated by adopt the Owens method[42] as follows:

$$\gamma_L(1+\cos\theta) = 2(\gamma_S^d \gamma_L^d)^{1/2} + 2(\gamma_S^p \gamma_L^p)^{1/2} \quad (2)$$

where, γ_S, γ_L, γ_S^d, γ_S^p, γ_L^d , γ_L^p are the surface free energy of the solid and

liquid, dispersion force term and polar force term of the solid, dispersion force term and polar force term of the liquid, respectively. The surface free energy of these liquid and their dispersion force term and polar force term are presented in **Table S1**.

2.7 DCMD set-up and membrane permeability

The desalination performance of the PVDF-CTFE membranes was evaluated using a laboratory-scale DCMD set-up (shown in **Fig. 1A**). Sodium chloride aqueous solution (35 g/L) and distillated water were used as the hot feed and cold permeate, respectively. The upper layer of membranes was contact with feed side and the supporting layer was contact with permeate side. Both side circulated with constant flow rate at 65 L/h and 50 L/h by magnetic pumps. The flat-sheet membrane module was consisted of two self-designed polymethyl methacrylate (PMMA) plate as shown in **Fig. 1B**. The flat-sheet membrane with an effective area of 5.218×10^{-3} m^2 was tightly clamped between the plates. The temperatures of both sides were kept at 55ºC and 25ºC. The concentration of sodium chloride in the distillate was monitored with an electric conductivity monitor. The permeate flux (J) was calculated using the following equation:

$$J = \frac{\mathrm{m}}{A \cdot \mathrm{t}} \tag{3}$$

Where J is the permeate flux [kg/(m^2.h)], m is the quantity of permeate (kg), A is the membrane effective area (m^2) and t represents the sampling time (h). The salt rejection coefficient R was calculated according to the following equation:

$$R = \frac{C_f - C_p}{C_f} \quad (4)$$

Where C_f and C_p are the salt concentrations of the feed and permeate, respectively.

Fig. 1

The sustainability of the hydrophobic membrane in DCMD process was also examined in this work using the same MD set-up with a 360 hrs continuous operation. The test was conducted under the same operation condition as in the permeate test, and the permeate flux and conductivity were recorded at set intervals.

3. Results and Discussion

3.1 Membrane morphology by SEM

The effects of molecular weight and dosage of PEG on the membrane micro-structure were systematically evaluated by FE-SEM images observation, as shown in Fig. 2 and Fig. 3.

Fig. 2

Fig. 2A and Fig. 2B clearly showed that the shape of the surface pores changed from circular to irregular and the interconnectivity increased along with the molecular weight of PEGs. Such an observation can be attributed to the phase inversion process because the formation of the top surface owing to the demixing of the casting solution by means of nucleation and growth of the polymer-rich phase[43]. Increased the molecular weight of PEGs, the casting solution became thermodynamically unstable and the viscosity became higher according to the entanglement of macromolecular

among polymer, solvent, and additive. As a result, the solution with lower mobility in the initial stage of immersion benefited the solid-liquid demixing (S-L) for the lower exchange rate of solvent and non-solvent. Which in turn encouraged the aggregation of the crystallites on membrane surface[44]. On the contrary, the use of low molecular weight PEG encouraged the fast exchange of solvent and non-solvent, thus leading to an instantaneous liquid-liquid demixing (L-L). That is, polymer crystallization process presented more influence as the molecular weight increased due to the decreasing phase inversion rate. The large circular pores found on the surface of membranes prepared using the lower molecular weight PEG was resulted from the L-L demixing during phase inversion, which was responsible for the formation of the enclosed and poorly interconnected pores. As PEGs with higher molecular weight were used, spheroidal crystallites was formed by S-L demixing (polymer crystallization) as shown **Fig. 2B**. As a result, irregular pores with higher interconnectivity was formed in membrane surface.

The cross-section of the PVDF-CTFE membranes containing PEGs additives with different molecular weight were showed in **Fig. 2C**. All membranes displayed a typical asymmetric structure consisting of a dense top layer, a number of macrovoids, and sponge-like sub-layer, which was typically formed during the L-L demixing process. Furthermore, it was observed that the size of the macrovoids expanded along with the increasing PEG molecular weight, which was in good agreement with previous studies [32, 33]. So it is safe to say that L-L demixing dominated the phase

inversion process for all the casting solution. However, the role of S-L demixing was increasingly important as the molecular weight increased due to the lower phase inversion rate as discussed for membrane surface. So the polymer crystals showed up in membrane cross-section and the pore interconnectivity was also significantly improved when using the PEGs with higher molecular weight. The phenomenon discovered in this work was in line with the previous work[34], they also demonstrated that the L-L demixing rate decreased and the S-L demixing started to take place when high molecular weight PEGs were used during the phase inversion process.

Fig. 3

The effect of PEG dosage on the membrane morphology was also investigated by FESEM as shown in **Fig. 3**. The pores on membrane surface became irregular and interconnected when increasing the dosage of PEG, and it was clearly that the number and size of the macrovoids in cross-section were firstly increased and then suppressed when increase the dosage of PEG. **Fig. 3D** further demonstrated that walls of pores including the macrovoids and the sponge-like layer were converted from imporous to open structure when increasing the PEG dosage, and the crystallites appeared when preparing the membranes with high PEG dosage. The morphology variation can also be attributed to the different phase inversion process induced by PEG. As the PEG dosage was lower than 3wt.%, the phase inversion rate increased as the dosage increased because the PEG which acted as additive would decreased the stability of casting solution and promote the exchange rate of solvent and non-solvent. As a result,

the membrane showed typical asymmetric structure in cross-section by instantaneous phase inversion. While as the dosage was higher than 5 wt.%, the thermodynamic effect showed greater influence which significantly increased the viscosity of casting solution. So the phase inversion rate decreased due to the lower exchange rate of solvent ant non-solvent. The delayed phase inversion process was benefit the S-L demixing, so the pores became irregular and the interconnectivity increased when further increase the PEG dosage as M2, M9, and M10 shown. Meanwhile, the phase inversion process induced by PEG with different dosage was also responsible for the two-stage promotion and suppression of the macro-voids in cross-section, as the instantaneous phase inversion was benefit the grow of macro-voids and vice versa.

3.2 Membrane surface roughness and pore structure

Fig. 4 showed the 3-D graphs and grayscale distribution of the membranes with different PEG dosage, the original 10,000× magnified SEM micrographs was shown in ***Fig. S3***. It can be found that the membrane roughness increased as the PEG dosage increased, this can be attributed to the crystals formed by the S-L demixing when more PEG was added. The grayscale histograms showed that the range of grayscale distribution became broader along with the PEG dosage, which also evidenced the increase of membrane roughness. The effect of PEG molecular weight on membrane surface 3-D morphology was also investigated as shown in ***Fig. S1***, with the original SEM image showed in ***Fig. S2***. The morphology and grayscale distribution showed slightly variation when the molecular weight was lower than 600 Da, while both

exhibited significantly increase when molecular weight was higher than 1000 Da (M4 and M5). This observation can be ascribed to the solution stability and viscosity due to the addition of higher molecular weight PEG additives.

Fig. 4

Table 2 showed the pore structure and roughness of the membrane surface, which was also obtained based on the SEM micrographs by image-pro-plus 6.0. It is clear that the surface porosity increased first but then decreased as the molecular weight was higher than 1000 Da when increase the molecular weight, however it increased along with the molecular weight for PEG dosage. The SEM roughness index showed good correlation with the surface 3-D morphology, i.e. increased along with the PEG molecular weight and dosage. The roundness of the surface pore was bigger when PEG with higher molecular weight or dosage was employed as compared to membrane with lower molecular weight or dosage, which means the pores shape altered bigger. However, the pore size showed no clear correlation with the PEG molecular weight or dosage which can be confirmed by **Fig.S1** and **Fig.S2**. The pore structure variation can also be explained by the phase inversion process during the membrane formation. As discussed in **section 3.1**, the S-L demixing imposed significant influence with the increased of PEG molecular weight and dosage, and the crystallization was beneficial for the formation of interconnected pore structure and rougher surface. The interconnected pore structure was benefit the surface porosity, roundness, and roughness. However, as the PEG additives with ultra-high molecular

weight were used (i.e. higher than 1000 Da), the polymer-rich phase dominated the surface composition. As a result, the porosity decreased as the membrane samples M4 and M5 showed. For surface pore size, it was influenced both by the porosity and the pore structure, these two opposite effects worked together which lead to the final pore size as can be found in Table 2 and related SEM graphs. In a word, the surface pore structure was totally affected by the phase inversion process which was influenced by PEGs with different molecular weight and dosage.

Table 2

3.3 Membrane hydrophobicity

The hydrophobicity was represented by the contact angle and surface free energy in this work, and the results were showed in **Table 3**.

Table 3

It was clearly evidenced that the hydrophobicity decreased when increasing the dosage of PEG, however the decreasing trend was reduced when more PEG was added. Correspondingly, the hydrophobicity firstly decreased as the molecular weight was lower than 600 Da and then increased when further increasing the molecular weight. On one hand, the addition of PEG was reported to decrease the hydrophobicity of membrane[41, 42]. On the other hand, the crystallites formed on the membrane surface due to the high dosage or molecular weight increased the membrane surface roughness, and thus leading to a higher hydrophobicity[47, 48]. These two contrary effect induced by PEGs with different molecular weight or dosage

worked together to the hydrophobic of the resultant membranes. As the molecular weight or dosage was relatively lower, the first factor played more important role which result in the decrease of hydrophobicity. While the later factor presents greater influence as the molecular weight or dosage increased, so the decreasing rate of hydrophobicity decreased or the increasing trend was observed when PEG-1000 or PEG-2000 was used due to its strong impact on membrane roughness. It was in agreement with the previous work when PEG was used for PVDF-HFP hydrophobic membrane preparation[49]. Such a variation was mainly believed to be caused by the variation in surface roughness due to the polymer crystallisation.

3.4 Porosity, pore size and pore distribution

The effect of PEG molecular weight and dosage on membrane overall porosity, pore size and pore size distribution were investigated and the results were showed in **Table 4** and **Fig. 5**. It was observed in **Table 4** that the membrane porosity was greatly improved when increasing the PEG molecular weight from 200 to 400 Da, while further increase in molecular weight only possessed slightly improvement. The membrane pore size also presents a similar trend. **Fig. 5A** showed that M2 and M4 presented the narrowest and broadest pore distribution, respectively. In terms of the effect of PEG dosage, it was noteworthy that the membrane prepared without PEG presented a slightly higher porosity than the membrane M7 due to the lowest relative polymer concentration as can be seen in **Table 4**. The overall porosity slightly increased as the dosage was lower than 5 wt.% and decreased as 7 wt.% PEG was

added, then re-increased when more PEG was added. Overall, the PEG dosage showed slightly influence on membrane overall porosity although the macrovoids of membrane by less than 5 wt.% dosage was larger. The higher pore interconnectivity of the membrane with higher PEG dosage was believed to offset the absence of macrovoids, and the higher porosity of M9 further verified this viewpoint. However, the pore size increased straight along with the PEG dosage and membranes with different dosage present narrow pore distribution as can be found in **Fig. 5B.**

Table 4

In a word, the addition of PEG influenced the membrane formation both thermodynamically and kinetically, which may result in both pore-forming and pore-inhibiting effect. The synergetic effect of these two opposite factors was responsible for the variation of membrane pore structure. Based on the results presented in **Table 4** and **Fig. 5**, it can be inferred that the PVDF-CTFE membrane containing 5 wt.% PEG-400 (M2) might offer excellent separation performance in MD desalination due to its moderate pore size and narrow pore distribution, as well as the interconnected pore structure pore structure as shown in **Fig. 3**.

Fig. 5

3.5 Membrane desalination performance

The permeability and rejection of resultant membranes in DCMD desalination was showed in **Fig. 6** in terms of the permeate flux, permeate conductivity, and the salt rejection. The salt rejection was nearly 100% when 5 wt.% PEG with different

molecular weights were used as shown in **Fig. 6A**. Whilst the permeate flux was greatly affected by the molecular weight of the additives, with M2 showing the highest water flux. It was in line with the morphological structure of the M2 membrane, which contained well-interconnected pore structure, moderate pore size and narrow pore size distribution.

Fig. 6

The PEG dosage also possessed significant impact on the membrane performance as shown in **Fig. 6B**. Interestingly, it was found that the permeate flux of M7 was slightly lower than M6, which was prepared without PEG addition. That can be explained by the higher hydrophobicity and porosity of membrane M6. However, the permeate flux was increased along with the PEG dosage, and the increasing rate was more pronounced in the lower dosage range (from 1 to 5 wt.%). It also should be noted that the membranes M9 and M10 were not suitable for the MD desalination process as a substantial decrease in salt rejection was observed due to the highest pore size as shown in **Fig. 5**.

PVDF-CTFE membrane with 5 wt.% PEG-400 was therefore considered as the candidate of choice for the MD process in the current study due to its interconnected pore structure, small pore size and narrow pore distribution, as well as the excellent desalination performance. The long-term operation performance of membrane M2 was then examined to demonstrate the sustainability performance of this membrane.

A 360 hrs continuous desalination experiment was carried out, and the separation results were shown in **Fig. 7**. The conductivity decreased quickly in the first 10 hrs, indicating a high permeate flux with low permeate conductivity had been offered. In the meantime, the permeate flux was maintained at approximately 18 kg/m^2.h during the first 50 hrs. Furthermore, the permeate flux remained almost constant at 18 kg/m^2.h during the entire period, with a marginal decline of less than 8%. Meanwhile, the permeate conductivity maintained lower than 13 μS/cm, although a slight increase trend was found 50 hrs later. The results shown in **Fig. 7** indicating that the PVDF-CTFE membranes prepared in this study exhibited stable long-term performance, and had great potential in MD process.

Fig. 7

3.6 Comparison with other hydrophobic membranes for MD

The DCMD performance of the membrane developed in this study was compared with other hydrophobic polymer membranes reported in recent years and the results were compiled in **Table 5**[50-62]. It can be found that the PVDF-CTFE membrane prepared in this work presented competitive advantages in permeate flux over other reported hydrophobic membranes at a temperature difference of 30 °C, which was 138.5% higher than PVDF membrane[53] and 23.4% higher than PVDF-HFP membrane[48]. While for salt rejection or permeate conductivity, the conductivity was 6 μS/cm (i.e, 99.98%) in this work, the PVDF-CTFE membrane also can be competitive as can be found in the **Table 5**. As to membrane sustainability, the membranes

prepared by PVDF-CTFE in the current study showed excellent performance as the permeate flux and the conductivity kept stable during the 360h continuous operation, which also showed competitive advantage to the comparison membranes. These results clearly suggested that the PVDF-CTFE copolymer was an excellent substitute for the preparation of hydrophobic membrane, because of the interconnected pore structure by crystallization, narrow pore distribution, and higher hydrophobicity. With careful tuning of the membrane properties using appropriate additives, these membranes showed great potentials in the MD applications.

Table 5

4. Conclusions

In this study, hydrophobic PVDF-CTFE membranes were prepared for MD desalination application. Effects of molecular weight and dosage of PEG additives were systematic studied in terms of membrane morphology, pore structure, hydrophobicity, and separation performance. It was revealed that the molecular weight and dosage of PEG have similar impact on membranes surface morphology and pore structure. The pores became irregular and interconnected while the surface porosity increased by the increasing molecular weight and dosage of PEG. In addition, the cross-section pore interconnectivity was also greatly improved with the increasing molecular weight and dosage of PEG. The effect of PEGs on phase inversion was responsible for the variation of membrane morphology and pore structure. The S-L

demixing possessed more important effect on membrane porosity, pore size, and pore interconnectivity with the increase of the molecular weight or dosage of PEGs. Increasing the molecular weight or dosage of PEG encouraged the formation of crystallites, which resulted in a rougher membrane surface, and increased the membrane hydrophobicity. It also worth to mention that all membranes displayed a water contact angles higher than 81.5°, which was suit for MD application.

The optimal membrane structure was found on the membrane with 5 wt.% PEG-400, which presents small pore size and narrow pore distribution, high hydrophobicity, especially the high interconnected pore structure which provide more passages for vapour transfer. A flux of 17.89 $kg/m^2.h$ with a rejection higher than 99.99% was achieved for this membrane. Long-term desalination test revealed that the PVDF-CTFE membrane with 5 wt.% PEG-400 delivered nearly constant permeation flux and salt rejection after 360 hrs continuous DCMD operation, indicating excellent performance sustainability of this membrane. This contribution clearly demonstrated that the PEGs with different molecular weight and dosage has significant influence on the resultant membranes mainly by the influence on phase inversion process, and the PVDF-CTFE hydrophobic membrane prepared in this work has great potential in DCMD desalination application due to the morphology, pore structure, properties variation induced by S-L demixing during membrane formation.

Acknowledgements

The authors was gratefully appreciate for the support by the National Science and Technology Major Project (No. 2012ZX07202006-03-2) and the National Natural Science Foundation of China (Grant NO. 51378491 and No. 51578533).

References

1 A. Subramani, J.G. Jacangelo, *Water Res.*, 2015, **75**, 164-187.
2 L.F. Greenlee, D.F. Lawler, B.D. Freeman, B. Marrot, P. Moulin, *Water Res.*, 2009, **43** , 2317-2348.
3 M. Elimelech, W.A. Phillip, *Science*, 2011, **333**, 712-717.
4 J.E. Miller, Review of water resources and desalination technologies, *Sandia national labs unlimited release report SAND-2003-0800*, 2003.
5 S. Burn, M. Hoang, D. Zarzo, F. Olewniak, E. Campos, B. Bolto, O. Barron, *Desalination*, 2015, **364**, 2-16.
6 E. Curcio, E. Drioli, *Sep. Purif. Rev*, 2005, **34**, 35-86.
7 A. Alkhudhiri, N. Darwish, N. Hilal, *Desalination*, 2012, **287**, 2-18.
8 P. Wang, T.S. Chung, *J. Membr. Sci.*, 2015, **474**, 39-56.
9 A. Alklaibi, N. Lior, *Desalination*, 2005, **171**, 111-131.
10 M. Khayet, *Adv. Colloid. Interfac.*, 2011, **164**, 56-88.
11 F. Liu, N.A. Hashim, Y. Liu, M.M. Abed, K. Li, *J. Membr. Sci.*, 2011, **375**, 1-27.
12 B. Ameduri, *Chem. Rev.*, 2009, **109**, 6632-6686.
13 Y. Yang, D. Rana, T. Matsuura, S. Zheng, C. Q. Lan, *RSC Adv.*, 2014, **4**, 38711-38717.
14 M. Qtaishat, D. Rana, T. Matsuura, M. Khayet, *AIChE J.* 2009, **55**, 3145-3151.
15 Z. Chen, D. Rana, T. Matsuura, Y. Yang, C. Q. Lan, *Sep. Purif. Technol.*, 2014, **133**, 303-312.
16 J. E. Efome, D. Rana, T. Matsuura, C. Q. Lan, *Water Res.*, 2016, **89**, 39-49.
17 Z. Cui, E. Drioli, Y.M. Lee, *Prog. Polym. Sci.*, 2014, **39**, 164-198.
18 F. Boschet, B. Ameduri, *Chem. Rev.*, 2013, **114**, 927-980.
19 J.H. Koh, Y.W. Kim, J.T. Park, J.H. Kim, *J. Polym. Sci. Pol. Phys*., 2008, **46**, 702-709.
20 J.H. Koh, J.A. Seo, J.T. Park, J.H. Kim, *J. Colloid. Interf. Sci*., 2009, **338**, 486-490.
21 Y.W. Kim, J.K. Choi, J.T. Park, J.H. Kim, *J. Membr. Sci.*, 2008, **313**, 315-322.
22 J.H. Koh, Y.W. Kim, J.T. Park, B.R. Min, J.H. Kim, *Polym. Advan. Technol.*, 2008, **19**, 1643-1648.

23 F. Liu, M.R.M. Abed, K. Li, *Chem. Eng. Sci.*, 2011, **66**, 27-35.
24 Y.W. Kim, J.T. Park, J.H. Koh, D.K. Roh, J.H. Kim, *J. Membr. Sci.*, 2008, **325**, 319-325.
25 H. Lee, M. Alcoutlabi, O. Toprakci, G. Xu, J.V. Watson, X. Zhang, *J. Solid. State. Electr.*, 2014, **18**, 2451-2458.
26 H. Lee, M. Alcoutlabi, J.V. Watson, X. Zhang, *J. Appl. Polym. Sci.*, 2013, **129**, 1939-1951.
27 J. Wang, L. Zheng, Z. Wu, Y. Zhang, X. Zhang, *J. Membr. Sci.*, 2016, **497**, 183-193.
28 Q.Z. Zheng, P. Wang, Y. N. Yang, *J. Membr. Sci.*, 2006, **279**, 230-237.
29 M. Khayet, C. Cojocaru, M. García-Payo, *J. Membr. Sci.*, 2010, **351**, 234-245.
30 G. Arthanareeswaran, D. Mohan, M. Raajenthiren, *J. Membr. Sci.*, 2010, **350**, 130-138.
31 Y.H. Zhao, B.K. Zhu, X.T. Ma, Y.Y. Xu, *J. Membr. Sci.*, 2007, **290**, 222-229.
32 S. Wongchitphimon, R. Wang, R. Jiraratananon, L. Shi, C.H. Loh, *J. Membr. Sci.*, 2011, **369**, 329-338.
33 J.H. Kim, K.H. Lee, *J. Membr. Sci.*, 1998, **138**, 153-163.
34 B. Chakrabarty, A. Ghoshal, M. Purkait, *J. Membr. Sci.*, 2008, **309**, 209-221.
35 A. Idris, N.M. Zain, M. Noordin, *Desalination*, 2007, **207**, 324-339.
36 G. De Silveira, P. Forsberg, T. Conners, S. Banerjee , *Surface analysis of paper*, 1995, 47-71.
37 G. Chinga-Carrasco, M. Lenes, P.O. Johnsen, E.L. Hult, *Micron*, 2009, **40**, 761-768.
38 S. Banerjee, R. Yang, C.E. Courchene, T.E. Conners, *Ind. Eng. Chem. Res.*, 2009, **48**, 4322-4325.
39 Z. Chen, D. Rana, T. Matsuura, D. Meng, C.Q. Lan, *Chem. Eng. J.*, 2015, **276**, 174-184.
40 Z. Chen, Study on Structure and Vacuum Membrane Distillation Performance of PVDF Composite Membranes: Influence of Molecular Weight and Blending, *University of Ottawa*, 2014.
41 C. Agarwal, A.K. Pandey, S. Das, M.K. Sharma, D. Pattyn, P. Ares, A. Goswami, *J. Membr. Sci.*, 2012, **415-416**, 608-615.
42 D.K. Owens, R. Wendt, Estimation of the surface free energy of polymers, *J. Appl. Polym. Sci.*, 1969, **13**, 1741-1747.
43 K. Kimmerle, H. Strathmann, *Desalination*, 1990, **79**, 283-302.
44 R. Boom, I. Wienk, T. Van den Boomgaard, C. Smolders, *J. Membr. Sci.*, 1992, **73**, 277-292.
45 S. Wongchitphimon, R. Wang, R. Jiraratananon, L. Shi, C.H. Loh, *J. Membr. Sci.*, 2011, **369**, 329-338.
46 Y.H. Zhao, B.K. Zhu, X.T. Ma, Y.Y. Xu, *J. Membr. Sci.*, 2007, **290**, 222-229.
47 M. Rafat, D. De, K. Khulbe, T. Nguyen, T. Matsuura, *J. Appl. Polym. Sci.*, 2006, **101**, 4386-4400.

48 Q. Li, Z.L. Xu, M. Liu, *Polym. Advan. Technol.*, 2011, **22**, 520-531.
49 Q.F. Alsalhy, K.T. Rashid, S.S. Ibrahim, A.H. Ghanim, B. Van der Bruggen, P. Luis, M. Zablouk, *J. Appl. Polym. Sci.*, 2013, **129**, 3304-3313.
50 C. Feng, B. Shi, G. Li, Y. Wu, *J. Membr. Sci.*, 2004, **237**, 15-24.
51 C. Feng, B. Shi, G. Li, Y. Wu, *Sep. Purif. Technol.*, 2004, **39**, 221-228.
52 C. Feng, R. Wang, B. Shi, G. Li, Y. Wu, *J. Membr. Sci.*, 2006, **277**, 55-64.
53 H. Fan, Y. Peng, *Chem. Eng. Sci.*, 2012, **79**, 94-102.
54 X. Wei, B. Zhao, X.M. Li, Z. Wang, B.Q. He, T. He, B. Jiang, *J. Membr. Sci.*, 2012, **407**, 164-175.
55 B.S. Lalia, E. Guillen-Burrieza, H.A. Arafat, R. Hashaikeh, *J. Membr. Sci.*, 2013, **428**, 104-115.
56 Y. Peng, Y. Dong, H. Fan, P. Chen, Z. Li, Q. Jiang, *Desalination*, 2013, **316**, 53-66.
57 D. Hou, H. Fan, Q. Jiang, J. Wang, X. Zhang, *Sep. Purif. Technol.*, 2014, **135**, 211-222.
58 Y. Liao, R. Wang, A.G. Fane, *Environ. Sci. Technol.*, 2014, **48**, 6335-6341.
59 L.D. Tijing, Y.C. Woo, M.A.H. Johir, J.S. Choi, H.K. Shon, *Chem. Eng. J.*, 2014, **256**, 155-159.
60 C. Yang, X.M. Li, J. Gilron, D.F. Kong, Y. Yin, Y. Oren, C. Linder, T. He, *J. Membr. Sci.*, 2014, **456**, 155-161.
61 A.K. Fard, Y.M. Manawi, T. Rhadfi, K.A. Mahmoud, M. Khraisheh, F. Benyahia, *Desalination*, 2015, **360**, 97-107.
62 M. Tian, Y. Yin, C. Yang, B. Zhao, J. Song, J. Liu, X.-M. Li, T. He, *Desalination*, 2015, **369**, 105-114.

List of tables

Table 1 Compositions of the polymer solutions for membrane casting.

Membrane code	M1	M2	M3	M4	M5	M6	M7	M8	M9	M10
Molecular weight of PEG	200	400	600	1000	2000	-	400	400	400	400
PEG concentration (wt.%)	5	5	5	5	5	0	1	3	7	9
DMAc concentration (wt.%)	83	83	83	83	83	88	87	85	81	79

Table 2 Pore structure and roughness of the membranes surface calculated by image-pro-plus 6.0.

Membenae code	Surface porosity (%)	Pore size (μm)			Roundness	SEM roughness index
		Max	Min	Mean		
M1	19.0	0.125	0.057	0.090	3.0	36.0
M2	20.7	0.128	0.054	0.091	3.2	38.0
M3	23.3	0.116	0.052	0.083	3.1	38.5
M4	22.2	0.138	0.053	0.093	3.9	42.0
M5	18.1	0.112	0.052	0.081	3.0	41.0
M6	10.5	0.132	0.062	0.094	3.0	26.9
M7	13.4	0.127	0.061	0.093	2.6	33.4
M8	20.7	0.115	0.052	0.083	3.2	37.6
M9	20.6	0.136	0.060	0.097	3.3	40.2
M10	24.1	0.149	0.056	0.099	3.5	43.4

Table 3 CA with different regents and the calculated surface free energy of the flat-sheet membranes.

Membrane code	CA_{water}(°)	$CA_{glycerol}$(°)	$CA_{diiodomethane}$(°)	γ(×10^{-5} N.cm^{-1})
M1	90.48±3.57	78.92±3.24	58.24±1.28	33.68±1.06
M2	87.30±4.08	76.83±1.62	55.32±1.75	36.10±1.64
M3	81.53±3.67	70.38±2.51	52.03±0.94	40.52±3.91
M4	83.11±3.10	71.52±3.27	54.23±2.42	38.98±3.71
M5	84.32±4.04	71.98±1.37	54.80±0.89	38.29±3.32
M6	92.58±3.18	80.26±2.16	59.53±1.37	32.34±0.70
M7	90.28±3.69	78.13±2.45	58.73±0.77	33.74±1.29
M8	87.32±3.14	77.03±1.38	56.75±0.98	35.55±1.95
M9	86.22±3.56	75.92±2.71	55.26±1.61	36.65±2.11
M10	86.36±1.59	76.38±0.86	54.76±0.62	36.83±2.12

Table 4 The overall porosity and pore size measured by Porometer Porolux 1000.

Membenae code	Overall porosity (%)	Pore size (μm)		
		Max	Min	Mean
M1	55.8±0.67	0.168±0.012	0.107±0.016	0.125±0.024
M2	65.5±0.79	0.234±0.030	0.105±0.005	0.132±0.015
M3	71.7±0.67	0.262±0.065	0.120±0.015	0.146±0.017
M4	72.5±0.74	0.217±0.051	0.092±0.012	0.137±0.035
M5	70.1±0.61	0.258±0.083	0.120±0.027	0.143±0.028
M6	63.1±0.67	0.164±0.045	0.078±0.016	0.088±0.021
M7	62.2±1.01	0.162±0.068	0.092±0.024	0.113±0.016
M8	67.1±0.52	0.178±0.066	0.081±0.002	0.130±0.032
M9	65.0±1.39	0.295±0.087	0.115±0.032	0.150±0.047
M10	65.4±0.66	0.486±0.125	0.121±0.056	0.174±0.043

Table 5 Comparison with other reported hydrophobic flat-sheet membranes by different polymer material in DCMD process.

Membrane	Feed solution			Permeate solution		Permeate flux ($kg/m^2.h$)	Salt rejection /permeate conductivity	Sustainability	Refs.
	Types[a]	Temp.[b] (℃)	Flux(L/h)	Temp. (°C)	Flux(L/h)				
PVDF-TFE	0.3 M	55	22	25	12	7.3	-	-	50
PVDF-TFE	0.3 M	55	22	25	12	2.5	100%	-	51
PVDF-HFP	0.3 M	55	50	25	12	14.5	>99%	30d, rejection kept higher than 90% .	52
PVDF(VIPS)	35 g/L	73	54	25	54	18.9	7.45 μS/cm	6h, flux decreased by 4.3%, rejection maintained at over 99.7%	53
PES (CF4 plasma modified)	4 %	63.3	0.36 m/s	20	0.36m/s	45.4	99.80%	55h, flux stayed around 39 kg/m^2 h after 40 h, then decreased to 36.4 kg/m^2 h; conductivity decreased from 7.81 to 7.45 μs/cm.	54
PVDF-HFP (electrospun)	10 g/L	65	900	24	900	22	98%	-	55
PSf (VIPS)	35 g/L	73	108	25	27	30	16 μS/cm	Feed flux change to 27°C 90h, flux decreased by 3.5%, conductivity maintain lower than 40 μS/cm.	56
PVDF	35 g/L	50	70	20	70	12.5	7.5	240h, flux maintain at 12.5 $kg/m^2.h$, conductivity stabilized at 5.3–7.5 μS/cm	57

PVDF-HFP	35g/L	60	48	20	48	18.9	<5 μS/cm	50h, flux maintained at 18.9 kg/m^2.h, conductivity lower than 5 μS/cm.	58
PVDF-HFP/PAN (electrospun)	DI water	60	24	20	24	45	>98.5%	-	59
[1]PVDF(CF4 plasma modified)	4 %	57.8	0.17 m/s	21.1	0.17 m/s	23.47	99.97%	-	60
[2]PVDF(Ar modified)						16.68			
PTFE	35g/L	70	180	30	180	32.5	99.90%	-	61
PSf (CF4 plasma modified)	DI	70.3	0.17	20	0.17	53.33	100%	27h, flux decreased by 10%, conductivity lower than 4 μS/cm.	62
PVDF-CTFE	35g/L	55	65	25	25	17.89	6 μS/cm	360h, flux decreased by less than 8%, conductivity kept lower than 13 μS/cm.	This work

Note: *a: The feed solution is NaCl solution which only the concentration is list if there is no detailed description; b: "Temp." represents the "temperature".*

List of figures

Fig. 5 Pore size distribution of the PVDF-CTFE membranes using PEG additives with (A) different molecular weight, and (B) different dosage.

Fig. 6 MD desalination performance of the PVDF-CTFE membranes using PEG additives with (A) different molecular weight, and (B) different dosage. (*Feed solution and temperature: 35 g/L NaCl solution, 55ºC; Permeate temperature: 25 ºC.*)

Fig. 7 Long-term desalination operation performance of the PVDF-CTFE membrane. (*Feed solution and temperature: 35 g/L NaCl solution, 55ºC; Permeate temperature: 25 ºC.*)

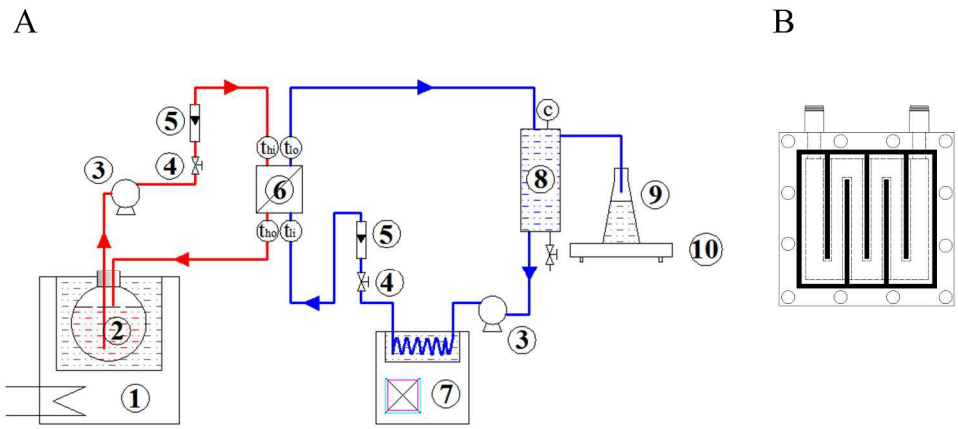

413x309mm (300 x 300 DPI)

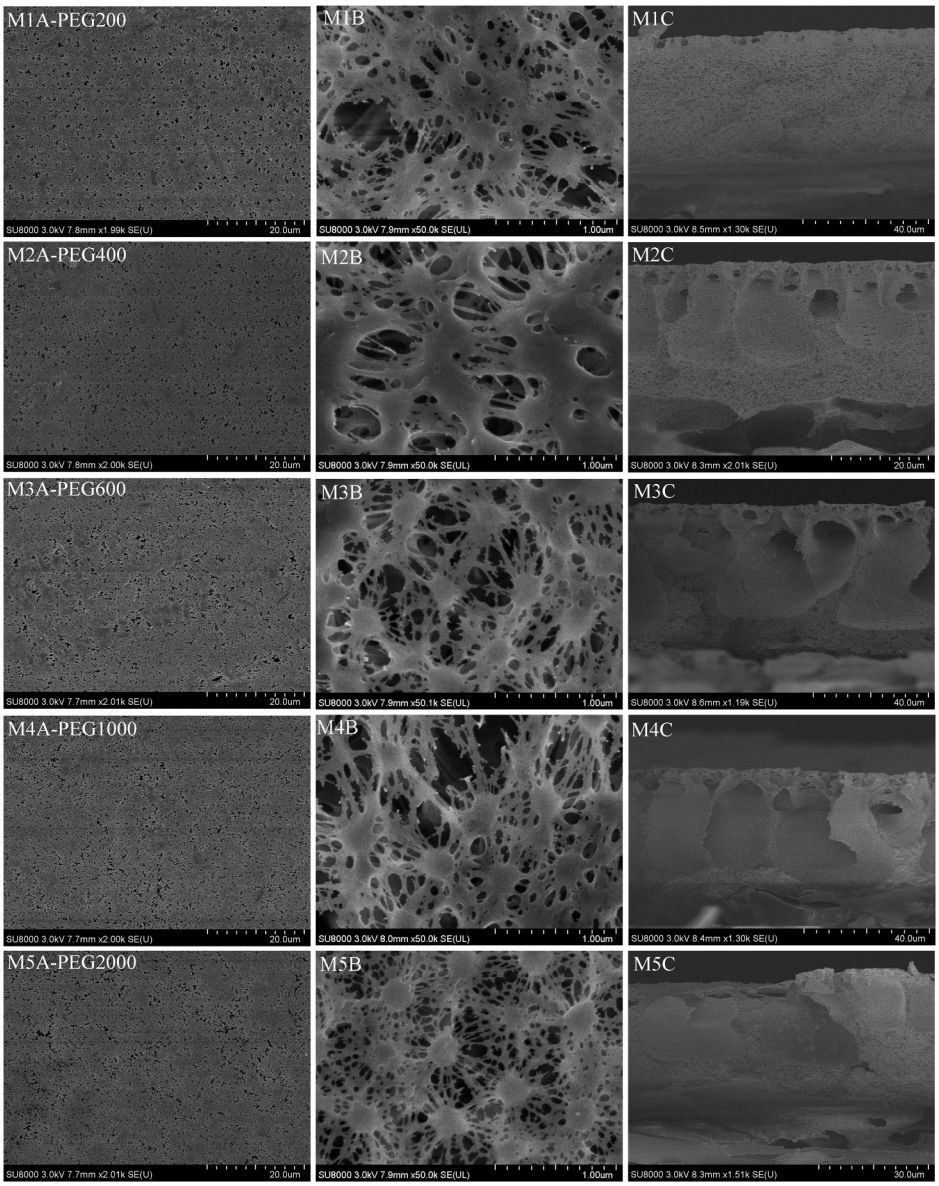

199x250mm (300 x 300 DPI)

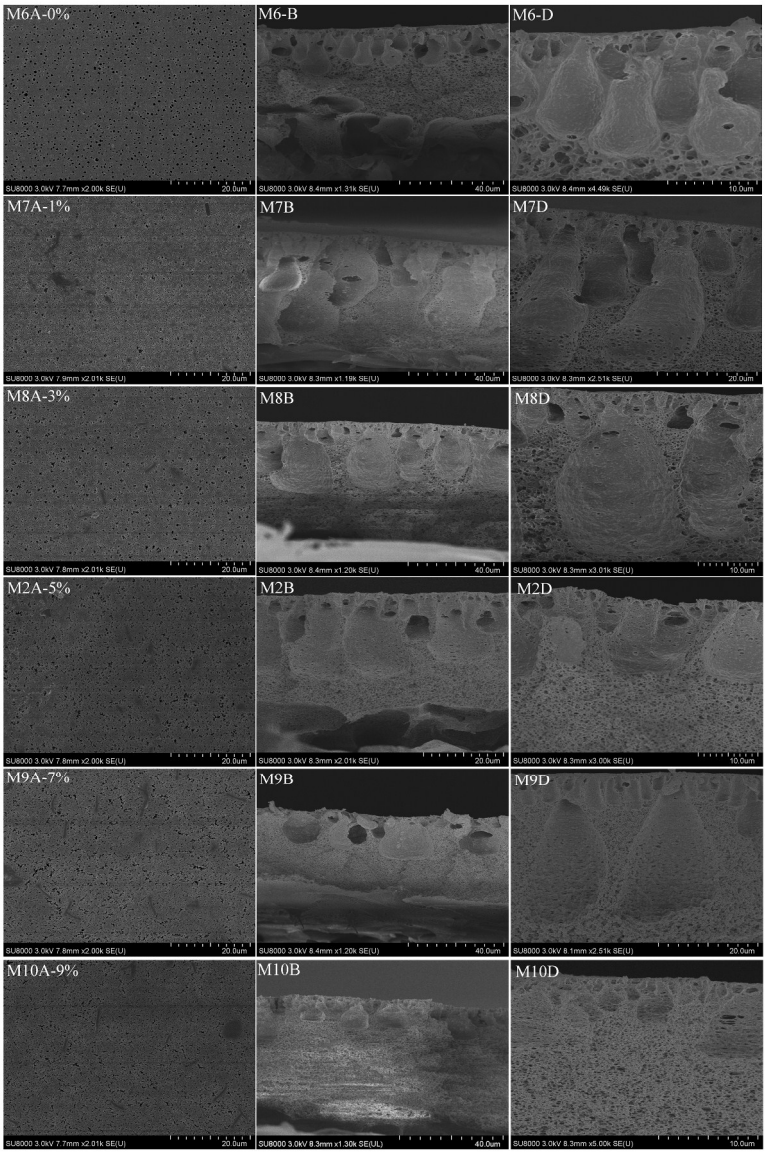

199x309mm (300 x 300 DPI)

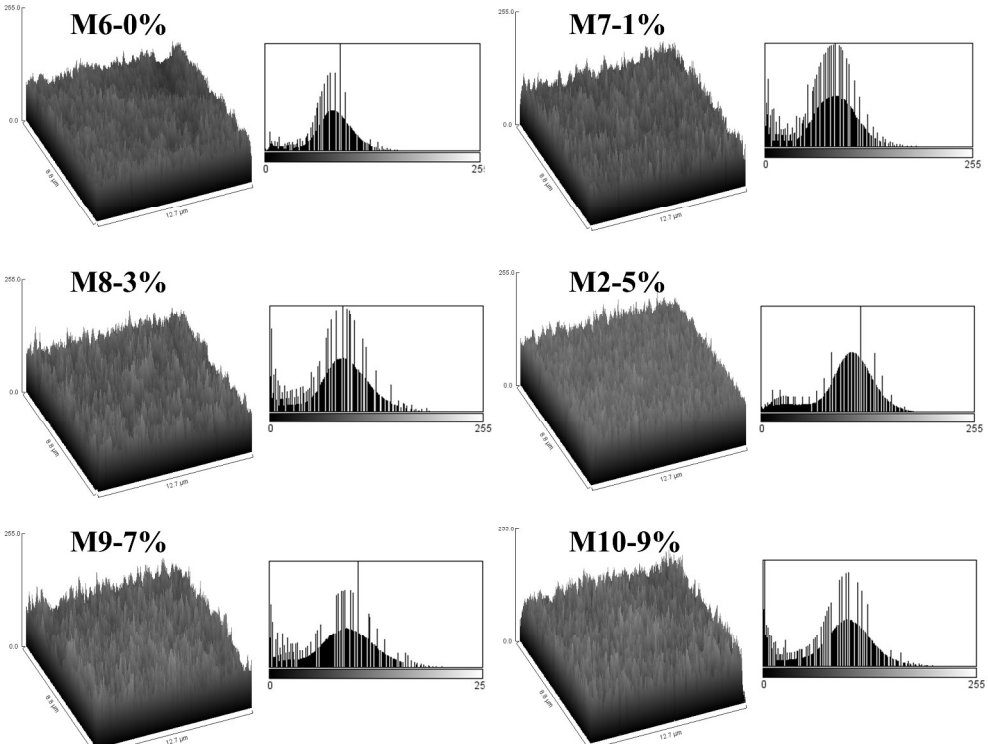

333x250mm (300 x 300 DPI)

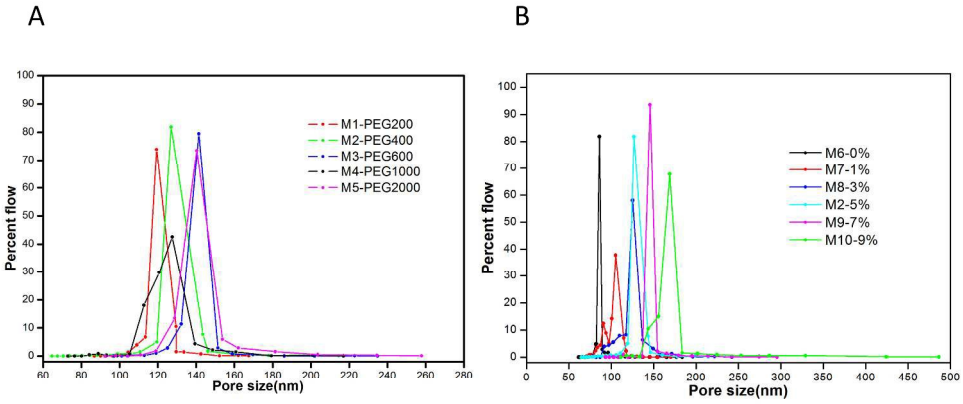

333x250mm (300 x 300 DPI)

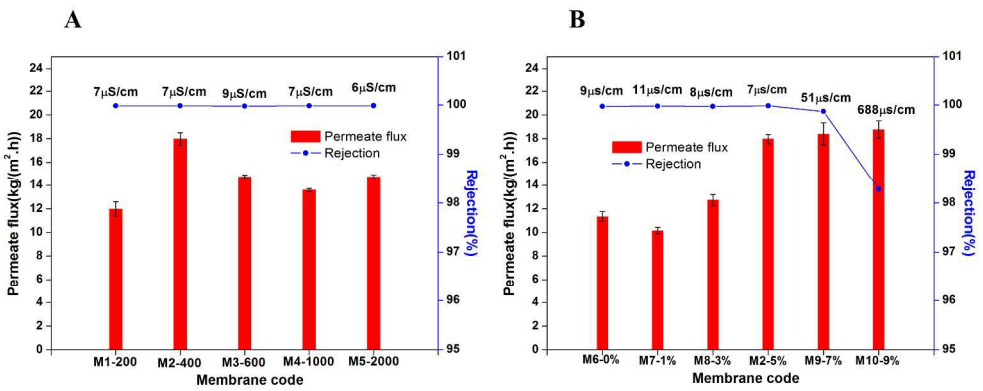

333x250mm (300 x 300 DPI)

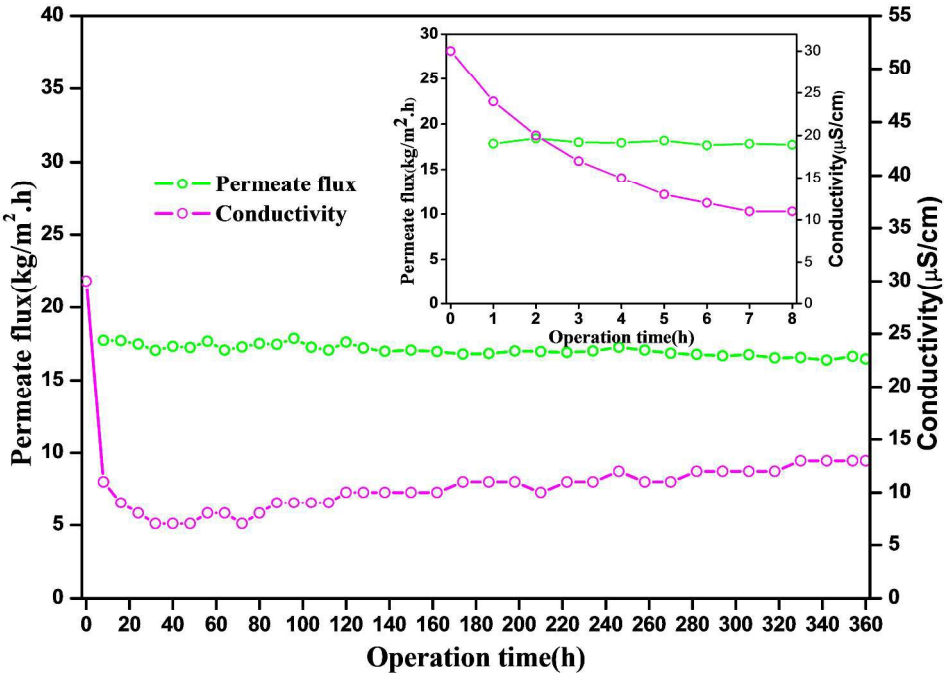

413x309mm (300 x 300 DPI)

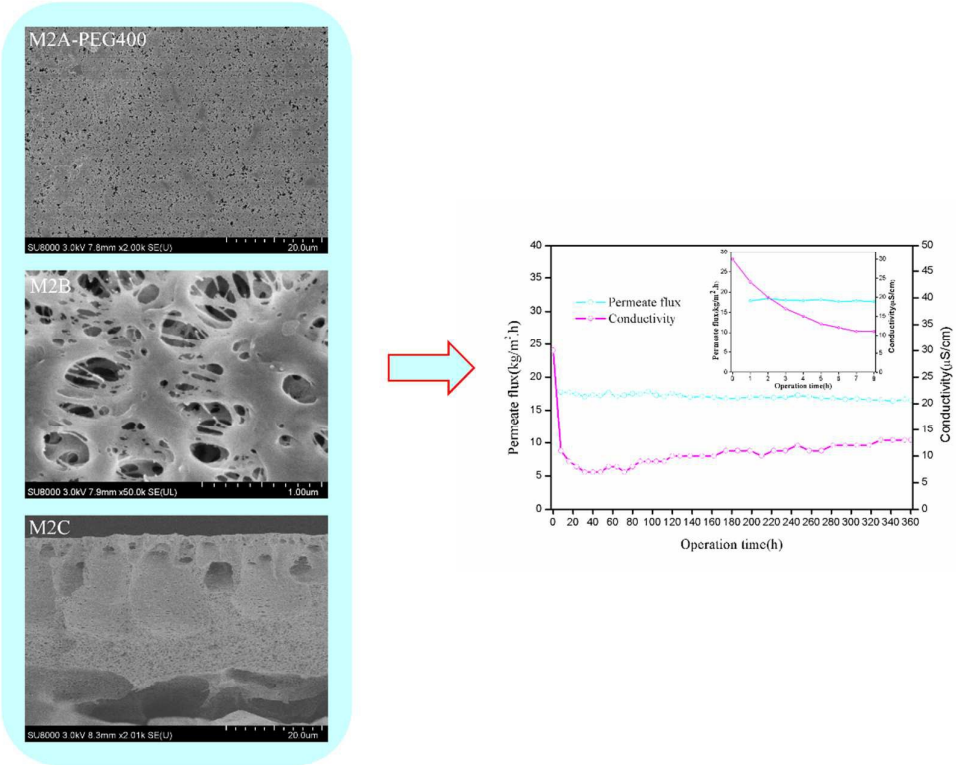

Figure. Graphical abstract

PVDF-CTFE membrane with interconnected pore structure, narrow pore distribution, and high DCMD performance was prepared by study the effect of molecular weight and dosage of PEG.